OPERATING CHARACTERISTICS OF THE SR5 HYPERSONIC PLASMA WIND-TUNNEL.

S. Mazouffre*[1], V. Caubet-Hilloutou[1], M. Dudeck[1], and E. Pawelec[2]

[1]Laboratoire d'Aérothermique, CNRS, 1c avenue de la Recherche Scientifique, 45071 Orléans, France.
[2]University of Opole, Oleska 48, Opole, Poland

ABSTRACT

The flow properties of a low-pressure weakly ionized supersonic argon plasma jet produced in the SR5 wind-tunnel are examined using Fabry-Pérot interferometry and Laser Induced Fluorescence spectroscopy. As expected, the plasma flow is found to be supersonic inside the divergent part of the arcjet nozzle. At the exhaust, the velocity reaches 4.5 km s^{-1} and the Mach number M is equal to 3.9. Surprisingly, the axial flow velocity measured along the jet centerline decreases down to about 3 km s^{-1} ahead of the stationary compression wave where $M = 4.8$. The on-axis velocity profile reveals the existence of several expansion cells that find their origin in the regular reflexion phenomenon, i.e. no Mach disk is formed. Hence, the supersonic to subsonic transition occurs far downstream. At the nozzle outlet, the parallel temperature is not in equilibrium with the perpendicular temperature: $T_{\parallel} \approx 4000$ K whereas $T_{\perp} = 1800$ K. The parallel temperature rises up to 5000 K in the shock region. Beyond the shock front both temperatures are in equilibrium: $T \approx 3000$ K.

Key words: SR5; plasma; supersonic flow; interferometry; LIF.

1. INTRODUCTION

The SR5 plasma wind-tunnel located at the Laboratoire d'Aérothermique in Orléans, France, is a ground-based facility that is employed to reproduce the environment encountered by a space probe in the course of its hypersonic entry stage in the upper layers of a planetary atmosphere. The facility consists of a large vacuum chamber and a vortex stabilized dc arc torch, which is equipped with a conical nozzle. A pumping system can ensure a residual pressure down to 1 Pa during operation. The facility enable the creation of steady high-enthalpy – several MJ kg^{-1} – plasma jets with different gas mixtures such as CO_2-N_2 (Mars), N_2-O_2 (Earth) and CH_4-N_2 (Titan). The SR5 plasma wind-tunnel offers two advantages over others experimental means like shock tubes (Boubert, 2002) and pulsed wind-tunnel (Mohamed, 2001): The easiness of probing the jet due to its large size and stationary flow conditions for several hours with a low level of contamination.

In order to characterize the SR5 facility in terms of flow velocity, streamline temperature and Mach number, a set of measurements have been performed when running the arcjet on argon seeded with a small amount of molecular nitrogen. Such an experiment can be considered as a test case, in the sense that the absence of a complex chemistry makes easier the understanding of the observed phenomena. The measurement campaign has been initiated in spring 2003, and preliminary experimental outcomes have been described in the works by Mazouffre (2003). In this contribution, we present and discuss the complete set of experimental results.

The accurate knowledge of the free plasma flow properties allows to clearly identify the part of the entry trajectory that can be simulated with the SR5 facility. Moreover, it allows to better define test conditions for the next series of experiments that will concern the study of rarefied supersonic flow around an obstacle.

A Fabry-Pérot interferometer has been used to obtain the plasma temperature and flow velocity in the direction of observation from the analysis of two Ar line profiles. A Laser Induced Fluorescence (LIF) spectroscopy technique based on a tunable laser diode has been employed to locally probe the velocity distribution function of Ar atoms from which both the velocity and the temperature are inferred.

In the contribution, the operating characteristics of the SR5 facility in terms of plasma temperature and velocity are critically reviewed after describing the wind-tunnel and the diagnostic techniques used to carry out experiments.

2. THE SR5 PLASMA WIND-TUNNEL

The plasma source used in the SR5 ground-test facility is a water-cooled vortex stabilized dc-arc torch

*To whom correspondence should be addressed: mazouffre@cnrs-orleans.fr

Table 1. Standard operating conditions.

Parameter	Value
I	100 A
U	45 V
$\dot{m}_{\mathrm{Ar}}$	0.26 g s^{-1}
$\dot{m}_{\mathrm{N_2}}$	0.04 g s^{-1}
p_{torch}	76 kPa
p_{chamber}	2.5 Pa

(Mazouffre, 2002). The torch is equipped with a tungsten cathode and with a convergent (60°)-divergent (50°) copper nozzle that acts as a grounded anode. The length of the divergent part is 5 cm and the exit diameter of the nozzle is 4.8 cm. The arc extends from the tip of the cathode through a 4 mm diameter molybden throat and attaches diffusely to the nozzle. The arcjet can be operated in a wide range of currents (10 to 300 A) and flows (5 to 50 slm). The plasma torch can be run for several hours, the lifetime being determined by the cathode erosion. Gases are fed through mass flow controllers directly into the cathode area. The torch is mounted on an arm that can be moved in vertical and horizontal direction. A thermal plasma is created in an Ar-N_2 gas mixture. Subsequently the plasma expands from the arcjet into a low pressure stainless steel vessel. The vacuum chamber is 4.3 m long and has a diameter of 1.1 m. The pumping system is made of three large Roots blower pump evacuated by a set of roughing pump. The capacity of the pump stack is 26000 m^3 h^{-1}, which ensures a residual pressure down to 1 Pa during operation. The pressure in the tank can, however, be changed almost independently from the gas flow by means of an adjustable valve. Standard operating conditions for this experiment are summarized in Table 1. The cathode to anode gap is 1 mm. The efficiency is around 65% and the specific enthalpy is 10.5 kJ g^{-1}.

A detailed description of the physics of rarefied supersonic plasma jets is available elsewhere (Miller, 1988). The plasma expanding through a nozzle from a high pressure region into a low pressure region, a well-defined free jet shock wave structure is produced. The plasma first flows supersonically: The Mach number reaches 1 at the nozzle throat and the flow is supersonic in the divergent section. In this flow domain, the temperature drops and the drift velocity increases due to energy conservation. In the mean time, the particle density along a streamline decreases because of the increase in the jet diameter, the so-called rarefaction effect. In case of an underexpanded jet, the flow domain is limited by a barrel shock wave behind the nozzle exit. At some distance from the source, depending among others upon the background pressure, the side shock waves interact with one another on the jet axis. Depending upon the exhaust Mach number and the rarefaction degree, two shock wave configurations are then possible as explained by Graur et al. (2000). A Mach disk associated with an oblique reflected shock can be created through which the flow undergoes a supersonic to subsonic transition: Mach reflection. Under specific conditions, the Mach disk may vanish and the flow experiences a supersonic to supersonic transition with a slight decrease in the Mach number magnitude: Regular reflection. The latter process can occur several times over appreciable distances leading to the appearance of several stationary expansion cells. Beyond the overall shock region, the plasma flows subsonically at constant static pressure. Deviation from the classical free jet flow picture may appear in the case of transient species like radicals and charged particles (Schram, 2001).

Table 2. On-axis conditions at the nozzle exhaust under our experimental conditions. The Ar density is obtained from the work of Kamińska (1999). λ refers to the local mean free path for momentum exchange.

Parameter	Value	Means
n_{Ar}	$\approx 10^{22}$ m^{-3}	Calculation
$\lambda_{\mathrm{Ar-Ar}}$	≈ 3 mm	Calculation
n_e	$\approx 10^{18}$ m^{-3}	Langmuir probe
T_{eq}	2250 K	LIF
v_z	4.5 km s^{-1}	LIF
M	3.9	LIF
h	10.1 kJ g^{-1}	Calculation

The value of some flow parameters under standard operating conditions are given in Table 2 at the torch nozzle exhaust[1]. As can be seen, the plasma is weakly ionized and the flow is in a transition regime with $Kn \approx 0.05$. The typical sizes of a jet produced in the SR5 wind-tunnel are: 0.2 m in diameter and about 1 m in length. The addition of a small fraction of molecular nitrogen to the argon gas flow simply permits to limit both the emission and the reabsorption of observed near infrared light. It has no influence upon the overall plasma flow characteristics. The efficient charge exchange reaction between Ar atoms and N_2^+ ions leads to the disappearance of a large number of Ar^+ ions, which are at the origin of the existence of excited Ar atoms as already explained by Mazouffre (2003).

3. OPTICAL DIAGNOSTIC TOOLS

3.1. Fabry-Pérot interferometry

The complete Fabry-Pérot interferometry bench has been extensively described in a previous paper (Mazouffre, 2003). We here briefly present the optical setup. The light emanating from the plasma is collected with a lens and transported towards the optical bench by means of a multimode optical fiber.

[1]The equilibrium temperature T_{eq} is given by $\frac{3}{2}kT_{\mathrm{eq}} = kT_{\perp} + \frac{1}{2}kT_{\parallel}$, where k is the Boltzmann constant. The specific enthalpy h is calculated as follows : $h = \frac{Cp}{M}T_{\mathrm{eq}} + \frac{v_z^2}{2}$, where Cp is the specific heat and M is the molar weight.

A similar fiber is also used to carry part of the light emitted by a low pressure argon lamp, which is used as a reference for null velocity. The two optical fibers are then combined into one. Subsequently, the light leaving the fiber coupler is collected with a lens in such a way that a collimated beam of light is created. The parallel beam passes a plane Fabry-Pérot cavity. Behind the cavity, the transmitted light is focused onto a pinhole in order to solely select the central interference ring. A monochomator acts as a rough wavelength selector to separate the line to be studied from the remainder of the spectrum. A photomultiplier tube (PMT) is used as a light detector. The Free Spectral Range of the cavity is equal to 9.924 GHz. In the wavelength region of interest, the FP setup allows to achieve a spectral resolution of about 0.15 GHz (0.4 pm).
Two configurations of the photon collection branch are available: The line of sight is oriented either at 90° or at 60° with respect to the jet symmetry axis. With the first configuration, one can measure the perpendicular temperature $T_\perp$ associated with the velocity distribution perpendicular to a stream line. Using the second configuration, one obtains the axial velocity component after correction with the cosine of the angle as well as the parallel temperature $T_\parallel$. Such a configuration allows to probe the plasma flow inside the nozzle of the arcjet. Fabry-Pérot spectroscopy does not allow to carry out measurements with a good spatial resolution. The field depth of the observation branch is around 25 cm, i.e. the field depth is as large as the plasma jet diameter. As a consequence, the obtained line profile corresponds to the one integrated along the line of sight, which prevents from measuring the radial velocity component as shown by Mazouffre (2003).
Two Ar line profiles are analyzed with the Fabry-Pérot setup. The Ar I line at 763.51 nm and the Ar I line at 738.40 nm. These two Ar lines offer several advantages: They are well isolated, they both correspond to a relatively strong transition, and the PMT quantum efficiency is relatively high below 800 nm. The temperature is deduced from the Doppler broadening of the line taking into account the apparatus width. The Doppler shift of the observed line allows to determine the mean velocity in the direction of observation.

3.2. Laser Induced Fluorescence

Since most of the experimental data presented in this paper originates in Laser Induced Fluorescence measurements, we choose to explain in detail the operation of the LIF spectroscopic tool. A schematic of the LIF optical bench is depicted in Fig. 1. A single mode tunable external cavity diode laser (SACHER TEC 500 in Littman configuration) delivers about 3 mW of horizontally polarized near-infrared radiation (800 nm to 830 nm) with a bandwidth of 0.5 MHz.
A Faraday isolator prevents any reflected beam of light to enter back into the laser cavity. A small fraction of the beam is passed through a low-pressure

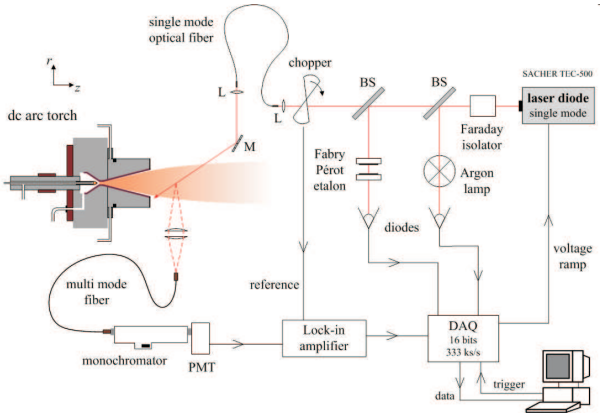

Figure 1. Schematic view of the experimental cw-LIF setup using a single mode tunable laser diode and phase sensitive detection. The laser beam can be directed either perpendicular or obliquely (at an angle of 30°) with respect to the flow direction. The map of the plasma plume properties is realized by moving the arcjet.

argon lamp. The absorption spectrum measured in that way is used to define the unshifted frequency position. A second beam splitter directs a small part of the laser into a 3.3 GHz Fabry-Pérot etalon to monitor mode structure and ensure that no mode hop occurs during operation. The mode-hop free tuning range of the laser is typically 30 GHz with voltage-current coupling. The recorded transmission of the Fabry-Pérot etalon is also used to linearize the frequency axis. The laser beam is coupled into a single mode optical fiber with a 5 μm core diameter using a 4 mm focal distance lens. Such a device allows to obtain a 30% coupling efficiency without shaping the beam. Two excitation configurations are possible. In one configuration using a plane gold mirror located inside the vacuum chamber, the laser beam propagates opposite to the plasma flow direction at a 30° angle with respect to the jet axis. In another configuration the beam is directed perpendicular to the flow direction. In both cases a 4 mm focal distance lens is used to focus the beam leaving the optical fiber onto the axis. The beam waist is estimated to be around 2 mm. The laser light is chopped at a frequency of about 750 Hz and the laser induced fluorescence signal is detected on a horizontal axis normal to both excitation directions. The signal is collected with two lenses (f_1 = 100 cm and f_2 = 20 cm) and imaged onto the entrance side of a 1 mm core diameter multimode optical fiber. The fiber is connected to a 20 cm focal distance monochromator centered at 810 nm with a bandwidth of about 0.5 Å in order to filter out extraneous plasma light. The 1 mm aperture of the fiber positioned at the focal plane of the imaging lens system determines the spatial resolution. The magnification is equal to 4, hence the resolution in horizontal direction is 4 mm. Phase-sensitive detection is used to discriminate the fluorescence light from the intrinsic plasma emission which is about 1000 times greater. The signal delivered by the PMT is analyzed with a lock-in amplifier which is synchronyzed to the chopper frequency. The current

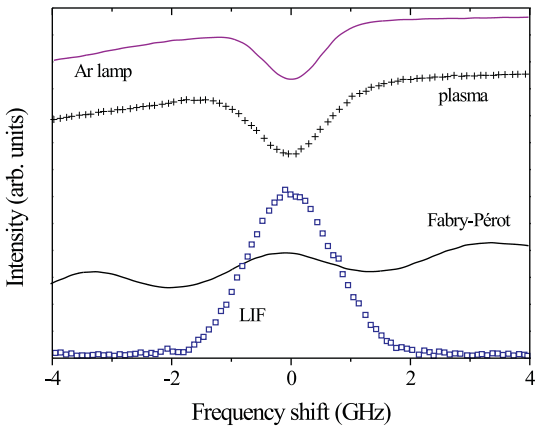

Figure 2. Raw waveforms obtained with the LIF diagnostic tool: absorption spectrum in a low pressure Ar lamp, absorption spectrum along the plasma jet diameter, transmission of the Fabry-Pérot etalon and fluorescence resulting from excitation of the Ar[1s$_4$] state in the plasma plume.

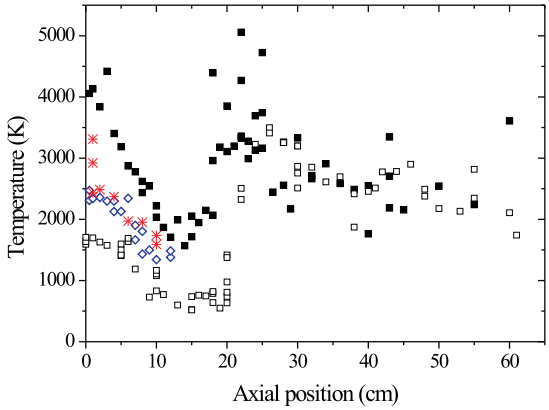

Figure 3. On-axis profile of the perpendicular temperature $T_\perp$ (open square) and the parallel temperature $T_\parallel$ (full square). The open diamond symbols correspond to experimental values of $T_\parallel$ obtained with a fresh cathode. The star symbols correspond to measurements carried out with a 0.065 $g\,s^{-1}$ N_2 mass flow rate.

integration time of the lock-in amplifier is 300 ms. All signals are recorded simultaneously with a 16 bit 333 kHz analog-to-digital converter (National Instruments PCI-6052E). The scanning of the laser frequency is controlled by supplying a low voltage to the piezoelectric block connected to the end mirror of the laser diode cavity. Typical scan times are several minutes.

All LIF measurements presented in this paper correspond to excitation of the Ar[1s_4] resonant level. The laser frequency is scanned over the $1s_4 \rightarrow 2p_7$ transition at 810.37 nm. Four raw waveforms obtained with the LIF diagnostic tool after radial excitation are shown in Fig. 2. As can be seen, the absorption spectrum across the plasma jet is similar to the absorption spectrum in a low pressure Ar lamp in terms of peak shape and position. It implies that the flow is axisymmetric. It also demonstrates that the jet can be used as a stationary reference for determining the zero Doppler shift. As shown in Fig. 2, the laser power varies during a scan over the Ar transition. LIF profiles must therefore be corrected in order to obtain the proper baseline. The bandwidth of the laser is in the order of 0.5 MHz, much narrower than the width of the measured Ar profiles. Both Stark broadening and pressure broadening can be neglected in view of, respectively, the low electron density and the low gas pressure. Furthermore, the saturation parameter S is found to be 0.03 for the concerned transition (Demtröder, 1998). Since S is much less than unity, the transition is not saturated meaning that the deposited laser power has no influence upon the Ar line shape. Hence, a recorded spectral profile is a direct measurement of the Ar atom velocity distribution function along the laser beam axis. The local mean Ar atom velocity is deduced from position of the fluorescence peak relative to the line measured in the argon lamp. If the system is in thermodynamic equilibrium, the Ar atom temperature is related to the width of the line.

4. TEMPERATURE ALONG THE JET CENTERLINE

The development along the jet centerline of the perpendicular temperature $T_\perp$, associated with the distribution function of the Ar atom radial velocity component – with respect to the jet axis – is shown in Fig. 3. Note that $z = 0$ corresponds to the nozzle exit. The temperature decreases due to the supersonic expansion of the plasma jet. The observed abrupt rise of $T_\perp$ indicates the presence of a stationary shock front through which kinetic energy is converted into thermal energy. Behind the shock, the temperature decreases due to the formation of secondary expansion domains, as explained in the next section. Far downstream when the Mach number M is below 1, the temperature decreases slowly due to energy exchange with the residual ambient gas.

The axial profile of the parallel temperature $T_\parallel$, associated with the distribution function of the Ar atom axial velocity component, is also shown in Fig. 3 for two different states of the plasma torch cathode. The lower value of the parallel temperature at the nozzle exit in the case of an unused cathode may arise from a difference in power deposition at the nozzle throat owing to a smaller anode to cathode distance[2]. The shape of the $T_\parallel$ profile resemble the one of $T_\perp$ and they are both directly connected to the jet shock wave structure. Across the shock front, the parallel

[2]Erosion of the cathode tip leads to an increase in the cathode to anode gap.

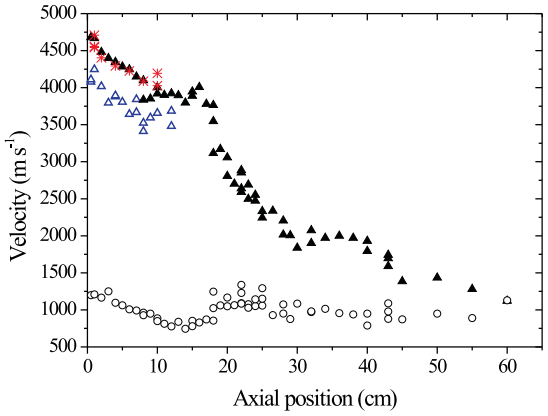

Figure 4. On-axis profile of the axial velocity component (triangle). The open diamond symbols correspond to experimental values of v_z obtained with a fresh cathode. The star symbols correspond to measurements performed with a 0.065 $g\,s^{-1}$ N_2 mass flow rate. Also shown is the speed of sound calculated from the measured parallel temperature (circle).

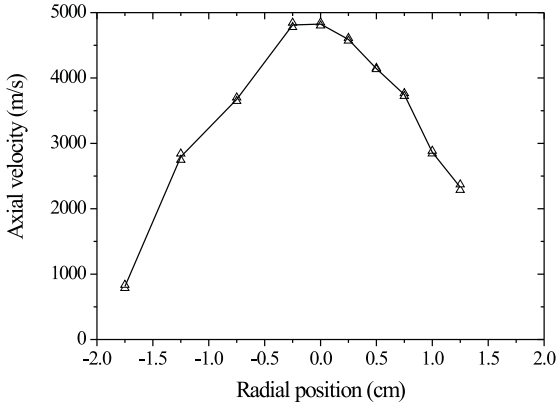

Figure 5. Radial profile of the axial velocity component measured by interferometry with the 738 nm Ar line inside the nozzle (z = -2 cm). As expected, the velocity is maximum on axis and it is zero close to the wall of the arcjet nozzle.

temperature rises up to 5000 K. Behind the shock region, the two temperatures are in equilibrium with of a value around 3000 K.
As can be seen in Fig. 3, the gap between $T_\parallel$ and $T_\perp$ is about 2500 K at the nozzle exit for a worn cathode. The departure from thermal equilibrium that occurs ahead of the shock region is a direct consequence of the rarefaction effect. At a certain station inside the divergent section of the nozzle the number of collisions becomes too low to maintain equilibrium between the two temperatures that quickly diverge from each other as the expansion process proceeds with $T_\perp < T_\parallel$ as explained by Miller (1969). Note that under our experimental conditions, the expansion process is not strong enough to permit the occurrence of the so-called frozen regime in which $T_\parallel$ stays constant whereas $T_\perp$ keeps on decreasing due to a purely geometrical effect (Miller, 1988). That means that behind the nozzle the collision frequency is still high enough to insure energy transfer in the core of the jet. As can be seen in Fig. 3, the temperature gradients along the jet centerline are very different: $\frac{\Delta T_\parallel}{\Delta z} = -225\ \mathrm{K\,cm^{-1}}$ and $\frac{\Delta T_\perp}{\Delta z} = -90\ \mathrm{K\,cm^{-1}}$. Surprisingly, the magnitude of the temperature gradients is contrary to expectation. Indeed, the supersonic expansion theory predicts that $\Delta T_\parallel < \Delta T_\perp$ in axial direction (Miller, 1988). The observed phenomenon is not yet well understood. However, a slight misalignement of the cathode – the cathode has been replaced between the measurement series – might well lead to a different flow dynamics through the nozzle, which in turn may influence the temperature profile. Notice that using Fabry-Pérot interferometry one finds about $-100\ \mathrm{K\,cm^{-1}}$ for the perpendicular temperature gradient (Mazouffre, 2003).

5. FLOW VELOCITY

5.1. Along the jet axis

The evolution of the axial velocity component v_z along the jet centerline is shown in Fig. 4. The on-axis velocity profile reveals the existence of several expansion cells that find their origin in the regular reflexion phenomenon: No Mach disk is formed, as explained by Graur (2000), and the flow undergoes a supersonic to supersonic transition across the standing shock wave with a Mach number reduction. The regular reflexion phenomenon is favored under our experimental conditions. Indeed, at the nozzle exit the Mach number is rather high ($M = 3.9$) and the rarefaction effect is already pronounced ($Kn \approx 0.05$). The present situation can be compared with previous experiments performed on underexpanding argon plasma jet at the University of Eindhoven by Engeln et al. (2000). In the latter situation, a straight nozzle was employed and the flow parameters at the exhaust were the following: $M = 1$ and $Kn \approx 2 \times 10^{-3}$. A Mach disk was found to be created through which the plasma flow did undergo a supersonic to subsonic transition, as predicted by Graur (2000).
Under our conditions, three standing shock waves are visible in Fig. 4 at $z = 0$ cm, $z \approx 18$ cm and $z \approx 40$ cm respectively. Consequently, three expansion cells are also defined. Throughout a standing shock wave the flow experiences a deceleration through a positive pressure gradient that originates in a compression effect (Miller, 1988). The decay in velocity that is observed at the nozzle exit, see Fig. 4, is the consequence of the existence of an oblique standing shock wave attached to the lip of the nozzle (Stern, 1960). This particular feature is observed for a fresh as well as a worn-out cathode. In order to cancel out any experimental artifact, a measurement series has been

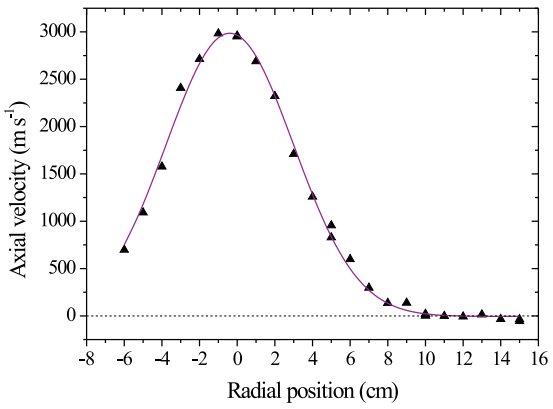

Figure 6. Radial profile of the axial velocity component measured at z = 10 cm. The jet boundary is located at r = 10 cm. The corresponding expansion half-angle is 33°.

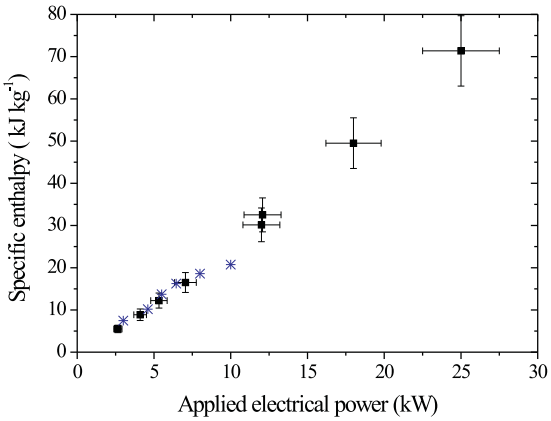

Figure 7. Specific enthalpy as a function of the applied electrical power: Calculated from the heat flux absorbed by the plasma torch (square); estimated from the measured axial velocity (star).

realized with a higher molecular nitrogen flow[3]. It appeared to be necessary to check whether the decrease in velocity observed at the torch outlet was not connected to a modification of the Ar atom velocity distribution function. Indeed, reabsorbtion of red shifted fluorescence light, which corresponds to slow atoms, along the observation path and the subsequent change in the velocity distribution may be errounously interpreted as a decrease in the local average drift velocity. The chosen conditions are the following: a 100 A direct current, a cathode-anode voltage of 55 V, an Ar gas flow of 0.26 $g\,s^{-1}$ and a N_2 gas flow of 0.06 $g\,s^{-1}$. The specific enthalpy is 10.4 $kJ\,g^{-1}$. The result of the experiment is shown in Fig. 4. As expected, the velocity decreases behind the nozzle exit. It clearly demonstrates that the observed trend is a real flow characteristics linked to the existence of an oblique shock wave. Notice that the added amount of N_2 is not large enough to lead to a global decrease in the velocity magnitude whatever the axial position. In other words, the amount of energy used for dissociating molecules and the fraction of energy stored in vibrational motion are not significant enough to influence the flow properties. This fact tends to prove that the nitrogen gas is fully dissociated. Similarly, the parallel temperature is not affected by a small change in the N_2 contents (see Fig. 3).

Measurements of the development of the axial velocity along the jet axis have also been carried out under standard conditions by means of Fabry-Pérot interferometry inside the nozzle as well as at the nozzle exhaust (Mazouffre, 2003). The velocity magnitude is in good aggrement with the one measured by LIF, however, the poor spatial resolution of the Fabry-Pérot setup does not allow to observe the decay in velocity at the nozzle exit.

[3]Increasing the seeded N_2 fraction leads to a decrease in the excited Ar atom contents, such atoms being at the origin of the reabsorption process of LIF photons (Mazouffre, 2003).

Also shown in Fig. 4 is the speed of sound calculated from the parallel temperature $T_{\|}$. The local speed of sound reads

$$c_s = \sqrt{\frac{\gamma k_B T_{\|}}{m}}, \qquad (1)$$

where γ is the specific heat ratio, k_B is the Boltzmann constant, and m is the mass of the specie. In case of a 4:1 Ar-N_2 mixture, $\gamma = 1.6$ and $m = 37.6$ amu. The speed of sound drops from 1.2 $km\,s^{-1}$ at the nozzle exit down to 0.8 $km\,s^{-1}$ ahead of the second shock front in the free flow domain. Note that throughout the paper, the Mach number M is defined as follows

$$M = \frac{v_z}{c_s(T_{\|})}. \qquad (2)$$

The Mach number is equal to 3.9 at the nozzle exit and $M = 4.9$ ahead of the second shock front at $z = 15$ cm. The plasma flow becomes subsonic at $z = 60$ cm, i.e. beyond the third shock wave.

5.2. Inside the nozzle

The radial development of the Ar atom axial velocity component has been measured inside the arcjet nozzle (z = -2 cm) by means of Fabry-Pérot interferometry, as can be seen in Fig. 5. As expected, the velocity is maximum on axis and the profile is symmetric. The velocity approaches zero close to the nozzle wall.

5.3. Across the plasma jet

The evolution of the axial velocity component measured by LIF along the plasma jet diameter at

$z = 10$ cm is shown in Fig. 6. The profile is perfectly symmetrical and it exhibits a bell-curve shape. The jet boundary – defined as the position for which $v_z = 0$ – is found to be located at $r = 10$ cm, which corresponds to an expansion half-angle of 33°. The temperature on-axis is around 1700 K and the temperature beyond the jet boundary (background gas) is 500 K.
The radial profile of the radial velocity component v_r measured by LIF at $z = 10$ cm has been presented in a previous article by Mazouffre et al. (2003). The velocity is null on the jet centerline and it reaches its maximum value (600 m s^{-1}) at $r = 3$ cm. It returns back to zero at $r = 8$ cm. It implies that from $r = 8$ cm to $r = 10$ cm the flow velocity is parallel to the jet center stream line, which is a feature of a barrel flow structure.

6. RANGE OF OPERATING CONDITIONS

An important parameter for this kind of plasma flows is the specific enthalpy (Lino da Silva, 2003). The enthalpy is directly linked to the applied electrical power, which in turn is connected to the gas composition. To a large extend, the specific enthalpy determines the maximum achievable velocity, which is a critical parameter when simulating supersonic entry conditions in a planetary atmosphere. In Fig. 7, the measured specific enthalpy h is plotted versus the supplied electrical power. The enthalpy is estimated from the measurement of the arcjet water cooling flow and temperature. As can be seen in Fig. 7, h varies linearly with the electrical power. The global yield increases from 60% at 2.5 kW to 85% at 25 kW. The enthalpy can also be calculated from the measured velocity. As can be seen in Fig. 7, the agreement between the two estimated values of h is good. It simply means that the energy is conserved along a streamline, as expected. The fact that the influence of the temperature upon h is negligible in the temperature range of interest is fully justified in view of the results.

The evolution of both the Ar atom axial velocity and temperature with the applied electric power is shown in Fig. 8. Measurements have been carried out inside the nozzle with the Fabry-Pérot bench (Mazouffre, 2003) The velocity as well as the temperature increase with the power whereas the Mach number stays approximately constant with a magnitude of about 3.5. The Ar atom temperature varies linearly with the supplied electric power contrary to the velocity.
As shown, by changing the power supplied to the plasma torch, one can change the range of achievable velocity. This is an interesting feature for ground-based simulation of entries in a planetary atmosphere. Indeed, it allows to simulate a large part of the entry trajectory. From our set of measurements, it follows that in the case of the SR5 facility, the velocity can reasonably be varied from 3 km s^{-1} to 8 km s^{-1} when operating the arcjet on argon. When

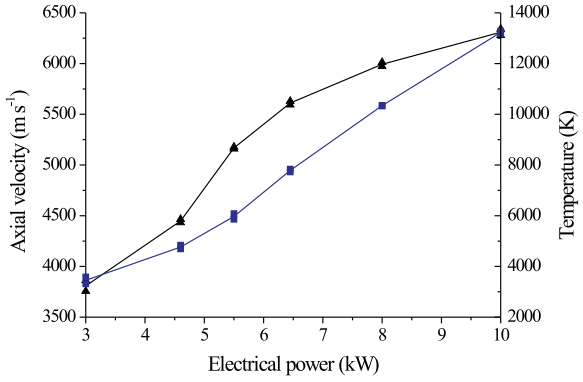

Figure 8. Temperature (square) and axial velocity (triangle) as a function of the applied electrical power. Measurements realized inside the nozzle (z = -2 cm) by monitoring the 738 nm Ar line profile with the FP interferometer. The temperature varies linearly with the power. The Mach number stays approximately constant ($M \approx 3.5$) whatever the power.

using molecular gases such as N_2 or CO_2 the velocity is expected to be smaller as part of the supplied energy is used for dissociation and stored in vibrational excitation. The lifetime of the arcjet is of course shortened when operating at high electric power.

7. CONCLUSION AND PERSPECTIVES

The flow properties of an underexpanding weakly ionized argon plasma jet produced in the SR5 wind-tunnel have been investigated using Fabry-Pérot interferometry and Laser Induced Fluorescence spectroscopy. The plasma flow is supersonic inside the divergent part of the torch nozzle. At the exhaust, the velocity reaches 4.5 km s^{-1} and the Mach number M is equal to 3.9. The axial velocity profile measured along the jet centerline reveals the existence of three expansion cells that result from the regular reflexion phenomenon. The first cell is believed to originate in the presence of an oblique shock wave attached to the lip of the nozzle. The on-axis flow velocity is equal to 3 km s^{-1} ahead of the second stationary compression wave where $M = 4.8$. Departure from thermal equilibrium is observed behind the nozzle exit – $T_{\parallel} > T_{\perp}$ – as the result of rarefaction. The parallel temperature rises up to 5000 K in the shock region.
In the SR5 ground-test facility, the flow velocity can be varied from 3 km s^{-1} to 8 km s^{-1} when running the torch with an atomic gas by changing the furnished electrical power. Therefore, the SR5 facility appears to be a perfectly suitable tool to simulate entry conditions of spacecrafts in the upper layers of planetary atmospheres.

In the near future, we plan to follow two research routes that are closely connected. First, as a direct

continuation of our current works, we will investigate the interactions between a rarefied supersonic argon plasma flow and an obstacle of various shape and material. Second, we will study the flow characteristics of a supersonic CO_2-N_2 plasma jet by means of LIF spectroscopy on excited oxygen atoms, in view of the simulation of space probe entry conditions in the Mars atmosphere.

ACKNOWLEDGEMENTS

The authors greatly appreciate the technical assistance of O. Antonin and P. Dom. The authors would like to acknowledge fruitful discussions with Dr. J.C. Lengrand and Dr. A. Lebéhot about underexpanding jet shock wave structure. This work was carried out with the support of the Région Centre.

REFERENCES

Boubert P., Chaix A., Chikhaoui A., Robin L., Vervish P., 2002, *Aerodynamic calibration of TCM2 facility and study of a bow shock layer by emission and laser spectroscopy.*, Shock Waves **11**, 341.

Demtröder W, 1998, *Laser Spectroscopy*, Springer, Berlin.

Engeln E., Mazouffre S., Vankan P, Schram D.C., Sadeghi N., 2001, *Flow dynamics and invasion by background gas of supersonically expanding thermal plasma*, Plasma Sources Sci. Technol. **10**, 595.

Graur I.A., Lengrand J.C., Elizarova T.G., 2000, *Numerical computation of shock wave configurations in underexpanded viscous jets*, Proceedings of the 22nd International Symposium on Shock Waves, London, UK, Edited by G.J. Ball, R. Hiller and G.T. Roberts, Vol. 2, 1267.

Kamińska A., Dudeck M., 1999, *Modelling of non-equilibrium arcjet plasma flow*, J. Tech. Phys. **40**, 33.

Lino da Silva M., Lago V., Reis. R, Dudeck M., 2003,*Modelling and experimental analysis of CO_2/N_2 plasma flows with and without the presence of an obstacle*, AIAA paper **03-3856**.

Mazouffre S., Pawelec E., Lago V., Lino da Silva M., Dudeck M., 2002, *Plasma formation during high speed flights in the upper layers of the Earth's atmosphere*, AIAA paper **02-5272**.

Mazouffre S., Pawelec E., Caubet-Hilloutou V., Dudeck M., 2003, *Experimental investigation of the flow properties of rarefied hypersonic plasma jets*, AIAA paper **03-3747**.
Both the Ar and N_2 gas flow cited in the AIAA paper are erroneous due to a bad calibration of the mass flow controllers. The correct values are the ones mentioned in the present article.

Miller D.R., Andres R.P., 1969, *Translational relaxation in low density supersonic jets*, Proceedings of the 6th Rarefied Gas Dynamics Symposium, Edited by L. Trilling and H.Y. Wachman, Vol. 2, 1385.

Miller D.R., 1988, *Free Jet Sources* in *Atomic and Molecular Beam Methods*, edited by G. Scoles, Oxford University, New York, 14.

Mohamed A.-K., Vérant, Soutadé J., 2001, *Infrared diode laser absorption spectroscopic characterisation on the free-stream in the F4 wind tunnel*, Proceedings of the 19th International Congress on Instrumentation in Aerospace Simulation Facilities, Cleveland, USA.

Schram D.C., Mazouffre S., Engeln R., van de Sanden M.C.M., 2001, *The physics of plasma expansions*, in Atomic and Molecular Beams, edited by R. Campargue, Springer, New York, 209.

Stern A.S., Waterman P.C., Sinclair T.F., 1960, *Separation of gas mixtures in a supersonic jet II*, J. Chem. Phys. **33**, 805.